

This is an Open Access document downloaded from ORCA, Cardiff University's institutional repository:<https://orca.cardiff.ac.uk/id/eprint/125176/>

This is the author's version of a work that was submitted to / accepted for publication.

Citation for final published version:

Braxton, Thomas M., Sarpong, Dionne Ea, Dovey, Janine L, Guillou, Anne, Evans, Ba , Castellano, Juan M., Keenan, Bethany E. , Baraghithy, Saja, Evans, Sam L. , Tena-Sempere, Manuel, Mollard, Patrice, Tam, Joseph and Wells, Timothy 2019. Thermoneutrality improves skeletal impairment in adult Prader-Willi syndrome mice. *Journal of Endocrinology* 243 (3) , pp. 175-186. 10.1530/JOE-19-0279

Publishers page: <http://dx.doi.org/10.1530/JOE-19-0279>

Please note:

Changes made as a result of publishing processes such as copy-editing, formatting and page numbers may not be reflected in this version. For the definitive version of this publication, please refer to the published source. You are advised to consult the publisher's version if you wish to cite this paper.

This version is being made available in accordance with publisher policies. See <http://orca.cf.ac.uk/policies.html> for usage policies. Copyright and moral rights for publications made available in ORCA are retained by the copyright holders.



1 **Thermoneutrality improves skeletal impairment in adult Prader-Willi syndrome**  
2 **mice**

3  
4 **Thomas M Braxton<sup>1</sup>, Dionne EA Sarpong<sup>1</sup>, Janine L Dovey<sup>1</sup>, Anne Guillou<sup>2</sup>,**  
5 **Bronwen AJ Evans<sup>3</sup>, Juan M Castellano<sup>4</sup>, Bethany E Keenan<sup>5</sup>, Saja Baraghithy<sup>6</sup>,**  
6 **Sam L Evans<sup>5</sup>, Manuel Tena-Sempere<sup>4,7</sup>, Patrice Mollard<sup>2</sup>, Joseph Tam<sup>6</sup> and**  
7 **Timothy Wells<sup>1\*</sup>**

8  
9 <sup>1</sup>School of Biosciences, Cardiff University, Museum Avenue, Cardiff, CF10 3AX, UK

10 <sup>2</sup>IGF, CNRS, INSERM, University of Montpellier, Montpellier, France

11 <sup>3</sup>School of Medicine, Cardiff University, Cardiff CF14 4XN, UK

12 <sup>4</sup>Physiology Section, Faculty of Medicine, University of Cordoba, and Instituto Maimonides  
13 de Investigacion Biomedica de Cordoba (IMBIC), 14004 Cordoba, Spain

14 <sup>5</sup>School of Engineering, Cardiff University, The Parade, Cardiff, CF24 3AA, UK

15 <sup>6</sup>Obesity and Metabolism Laboratory, Institute for Drug Research, School of Pharmacy,  
16 Faculty of Medicine, The Hebrew University of Jerusalem 9112001, Israel

17 <sup>7</sup>CIBER Fisiopatologia de la Obesidad y Nutrición (CIBEROBN), Instituto de Salud Carlos  
18 III, 14004 Cordoba, Spain

19

20

21 **Running head: Skeletal Phenotype in PWS-IC<sup>del</sup> Mice**

22 **Word Count: 4986** (including the Abstract)

23 **\*Author for correspondence:**

24 Dr Timothy Wells  
25 School of Biosciences,  
26 Cardiff University,  
27 Cardiff. CF10 3US, UK  
28 Tel: (+44) 2920 874977  
29 Fax: (+44) 2920 876328  
30 E-mail: [wellst@cardiff.ac.uk](mailto:wellst@cardiff.ac.uk)

31 **Abstract**

32 Human Prader-Willi syndrome (PWS) is characterised by impairments of multiple  
33 systems including the growth hormone (GH) axis and skeletal growth. To address our  
34 lack of knowledge of the influence of PWS on skeletal integrity in mice, we have  
35 characterised the endocrine and skeletal phenotype of the PWS-IC<sup>del</sup> mouse model for  
36 “full” PWS and determined the impact of thermoneutrality.  
37 Tibial length, epiphyseal plate width and marrow adiposity were reduced by 6%, 18%  
38 and 79% in male PWS-IC<sup>del</sup> mice, with osteoclast density being unaffected. Similar  
39 reductions in femoral length accompanied a 32% reduction in mid-diaphyseal cortical  
40 diameter. Distal femoral Tb.N was reduced by 62%, with individual trabeculae being  
41 less plate-like and the lattice being more fragmented (Tb.Pf increased by 63%). Cortical  
42 strength (Ultimate moment) was reduced by 26% as a result of reductions in calcified  
43 tissue strength and the geometric contribution. GH and prolactin contents in PWS-IC<sup>del</sup>  
44 pituitaries were reduced in proportion to their smaller pituitary size, with circulating IGF-1  
45 concentration reduced by 37-47%. Conversely, while pituitary LH content was halved,  
46 circulating gonadotropin concentrations were unaffected. Although longitudinal growth,  
47 marrow adiposity and femoral geometry were unaffected by thermoneutrality,  
48 strengthened calcified tissue reversed weakened cortex of PWS-IC<sup>del</sup> femora.  
49 While underactivity of the GH-axis may be due to loss of *Snord116* expression and  
50 impaired limb bone geometry and strength due to loss of *Mage12* expression,  
51 comprehensive analysis of skeletal integrity in the single gene deletion models is  
52 required. Our data imply that thermoneutrality may ameliorate the elevated fracture risk  
53 associated with PWS.

## 54 Introduction

55 Prader-Willi syndrome (PWS) is a neurodevelopmental disorder arising from the loss of  
56 expression of one or more genes from the paternal allele of the PWS locus (Butler *et al*,  
57 2016). The PWS phenotype is complex, characterised by neonatal hypotonia and an  
58 initial failure to thrive (Miller *et al*, 2011), the subsequent development of hyperphagia  
59 (Miller *et al*, 2011), hyperghrelinemia (Cummings *et al*, 2002), and growth hormone  
60 (GH) deficiency (Grosso *et al*, 1998), resulting in severe truncal obesity and growth  
61 retardation (Kahn *et al*, 2018).

62

63 By manipulating the murine PWS locus on chromosome 7, several mouse models for  
64 this condition have linked the contribution of individual PWS genes to specific phenotypic  
65 characteristics. For example, while loss of the *MAGE*-family gene, *Necdin* has no effect  
66 on growth or adiposity (Cattanach *et al*, 1992, Muscatelli *et al*, 2000) *Necdin*-null mice  
67 display enhanced differentiation and/or proliferation of astrocytes (Fujimoto *et al*, 2016),  
68 neocortical neural precursor cells (Minamide *et al*, 2014), hematopoietic stem cells (Asai  
69 *et al*, 2012) and pre-adipocytes (Fujiwara *et al*, 2012). Similarly, although deletion of  
70 another *MAGE*-family gene, *Mage12*, fails to induce hyperphagia with standard diets  
71 (Bischof *et al*, 2007), *Mage12*-null mice display impaired GH axis function (Tennese &  
72 Wevrick, 2011) and leptin sensitivity (Pravdivyi *et al*, 2015), accompanied by a doubling  
73 of fat mass (Bischof *et al*, 2007). In contrast, loss of the small nucleolar (sno)RNA,  
74 *Snord116*, results in mild hyperphagia and impaired meal-termination, but accompanied  
75 by intra-abdominal leanness (Ding *et al*, 2008).

76

77 Such studies have revealed features of PWS not commonly reported in humans. For  
78 example, our study of metabolic homeostasis in the PWS-IC<sup>del</sup> mouse, in which paternal  
79 inheritance of an imprinting centre (IC) deletion results in a complete lack of gene

80 expression from the entire PWS interval ([Chamberlain \*et al\*, 2004](#)), revealed overactive  
81 brown fat and excess heat production ([Golding \*et al\*, 2017](#)). Unlike humans with PWS  
82 ([Kahn \*et al\*, 2018](#)), PWS-IC<sup>del</sup> mice display profound abdominal leanness, probably  
83 resulting from a compromised capacity of PWS adipocytes to import lipid ([Golding \*et al\*,](#)  
84 [2017](#)), a phenomenon reported in isolated human PWS adipocytes ([Cadoudal \*et al\*,](#)  
85 [2014](#)).

86

87 Disruption of adipocyte function has extra-metabolic consequences. For example, there  
88 is a bi-directional relationship between fat and bone ([Leiben \*et al\*, 2009](#)), with bone  
89 marrow adipocytes and the bone-forming osteoblasts arising from the same  
90 mesenchymal stem cells (MSCs) ([Beresford \*et al\*, 1992](#), [Di Iorgi \*et al\*, 2008](#)) and  
91 osteogenesis being influenced by leptin ([Thomas \*et al\*, 1999](#), [Hamrick \*et al\*, 2005](#), [Evans](#)  
92 [\*et al\*, 2011](#)). Although several studies have examined the effects of the loss of specific  
93 PWS interval regions/genes on bone ([Khor \*et al\*, 2016](#), [Kamaludin \*et al\*, 2016](#),  
94 [Baraghithy \*et al\*, 2019](#)), a study of the impact of losing all of the genes in the PWS locus  
95 is lacking. We have therefore conducted a study of the growth, morphology,  
96 microarchitecture and biomechanical properties of the appendicular bones of PWS-IC<sup>del</sup>  
97 mice and characterised the underlying endocrine phenotype. In addition, since we have  
98 recently shown that maintaining PWS-IC<sup>del</sup> mice at thermoneutrality may reduce  
99 proportionate hyperphagia ([Golding \*et al\*, 2017](#)), we quantified the effect of this  
100 manipulation on bone morphology and strength.

## 101 **Materials and Methods**

102

### 103 *Animals*

104 The mice used in this study were bred under the authority of the Animals (scientific  
105 procedures) Act 1986 (UK), with subsequent procedures conforming with the ARRIVE  
106 guidelines and specifically approved by the Cardiff University Animal Welfare Ethical  
107 Review Body (AWERB).

108

109 PWS-IC<sup>m+/p-</sup> (referred to throughout as PWS-IC<sup>del</sup>) and wild-type (WT) littermates were  
110 generated by crossing IC<sup>del</sup>-positive males with WT females. Given that PWS-IC<sup>del</sup>  
111 animals on a pure C57BL/6J background suffer severe postnatal lethality (Yang et al,  
112 1998), we crossed IC<sup>del</sup> positive males with CD1 females and selectively culled WT  
113 littermates (identified on the basis of their increased size 48 hours after birth) leaving  
114 only 1 or 2 WT pups per litter (Chamberlain et al, 2004). Animals were weaned at  
115 approximately 4 weeks of age and housed in single-sex groups with WT littermates (2-5  
116 animals per cage).

117

118 All animals were maintained on a 12hr light/dark cycle (lights on 07:00h) at 20-22°C  
119 (unless otherwise stated), with *ad libitum* access to water and standard laboratory chow  
120 (Rat and Mouse No. 3 Breeding Diet, Special Diet Services Ltd., Witham, Essex, UK,  
121 containing 4.2% crude fat; 22.4% crude protein; 4.2% crude fibre; 7.6% crude ash (see  
122 Tilston et al, 2019 for full dietary composition).

123

### 124 *Study 1. Tibial growth and marrow adiposity in PWS-IC<sup>del</sup> mice*

125 After an overnight fast (with water available *ad libitum*), 18-month old male PWS-IC<sup>del</sup>  
126 and WT littermates were killed by cervical dislocation. Left tibiae were excised, the

127 length determined with a hand-held micrometer and fixed in buffered formal saline for  
128 48hrs at 4°C before being decalcified in 0.5M EDTA (pH 7.6). Tibiae were stored in 70%  
129 ethanol at 4°C prior to quantifying epiphyseal plate width (EPW), marrow adiposity and  
130 osteoclast number (see below).

131

### 132 *Study 2. Femoral phenotype in PWS-IC<sup>del</sup> mice*

133 Left femora were excised from the mice in study 1, soft tissue removed and length  
134 measured with a hand-held micrometer. Femora were wrapped in saline-soaked gauze,  
135 snap frozen and stored at -80°C for subsequent  $\mu$ -CT and biomechanical analysis (see  
136 below).

137

### 138 *Study 3. Endocrine status in PWS-IC<sup>del</sup> mice*

139 Male and female PWS-IC<sup>del</sup> and their 6-15-month old WT littermates were anaesthetised  
140 with isoflurane and killed by decapitation. Pituitaries were dissected, weighed, snap  
141 frozen and stored at -80°C for subsequent quantification of growth hormone (GH),  
142 prolactin (PRL) and luteinising hormone (LH) content (see below).

143

144 Male and female PWS-IC<sup>del</sup> and their 5-9-month old WT littermates were anaesthetised  
145 with isoflurane and killed by decapitation. Pituitaries were dissected and weighed and  
146 trunk blood collected into EDTA-coated tubes, vortexed and centrifuged. Aliquots of  
147 separated plasma were snap frozen and stored at -80°C for subsequent quantification of  
148 circulating insulin-like growth factor-1 (IGF-1), LH and follicle stimulating hormone (FSH)  
149 (see below).

150

### 151 *Study 4. The effect of thermoneutrality on skeletal parameters in PWS-IC<sup>del</sup> mice*

152 Male and female PWS-IC<sup>del</sup> and their 6-15-month old WT littermates were group-housed  
153 in standard mouse cages (2-3 mice /cage) at 20-22°C or at thermoneutrality (30°C)  
154 (Golding *et al*, 2017). After 9 weeks, mice were anaesthetised with isoflurane and killed  
155 by decapitation. Tibiae and femora were excised and processed as above (studies 1 &  
156 2) for subsequent quantification of growth, adiposity, geometry and strength.

157

#### 158 *Quantification of tibial epiphyseal plate width and marrow adiposity*

159 Tibial EPWs and marrow adiposity were measured as previously described (Gevers *et*  
160 *al*, 2002; Thompson *et al*, 2004, Navein *et al*, 2016, Hopkins *et al*, 2017). In brief, three  
161 7µm anterior-posterior longitudinal tibial sections were stained with Masson's Trichrome  
162 and visualised under light microscopy. Total plate width was measured in triplicate on  
163 digitally captured images of each section using the interactive feature tool of Leica QWin  
164 (V3.2). Marrow adiposity was quantified on digital images of mid-diaphyseal marrow and  
165 photomicrographs analysed with National Institutes of Health (NIH) Image J, to quantify  
166 %-adiposity, and the number and size of marrow adipocytes.

167

#### 168 *Quantification of tibial osteoclasts*

169 To identify osteoclasts, consecutive paraffin sections were de-paraffinised, stained for  
170 tartrate-resistant acid phosphatase (TRAP; Sigma-Aldrich), and counterstained with  
171 Mayer's haematoxylin. Histomorphometric analysis was performed on digital  
172 photomicrographs using IMAGE-PRO PLUS V.6 (Media Cybernetics, Silver Spring, MD)  
173 to determine the number of TRAP<sup>+</sup> osteoclasts per bone surface (N.Oc/BS).

174

#### 175 *Quantification of femoral trabecular architecture*

176 The trabecular microarchitecture of the distal femora was assessed using a high-  
177 resolution µ-CT system (Bruker Skyscan 1272, Kontich, Belgium) as previously

178 described in rats (Evans *et al*, 2011) and mice (Navein *et al*, 2016). Femora were  
179 thawed, mounted on the sample presentation stage and orientated by taking a series of  
180 single images. Scanning was conducted at 70kV and 142 $\mu$ A, using a resolution of  
181 9.04 $\mu$ m, 990 millisecond exposures, a rotation step of 0.60° and a 0.5mm aluminium  
182 filter. Analysis was performed according to the ASBMR guidelines (Bouxsein *et al*,  
183 2010). In brief, a 1mm<sup>3</sup> ROI of secondary spongiosa 0.5mm above the centre of the  
184 distal epiphyseal plate was analyzed using the CT image analysis software (CT-An;  
185 <https://www.bruker.com/products/microtomography/micro-ct-software/3dsuite.html>).  
186 Trabecular bone was separated from cortical bone within the area of interest by using  
187 the freehand drawing tool in CT-An. After scanning, femora were re-wrapped in saline-  
188 soaked gauze and re-frozen and for strength testing.

189

#### 190 *Biomechanical testing*

191 Mechanical strength of the femoral cortex was quantified by three-point bending as  
192 previously described (Stevenson *et al*, 2009, Navein *et al*, 2016), with the lower rollers  
193 set at 6.42 and 4.04 mm apart for WT and PWS-IC<sup>del</sup> femora respectively and the central  
194 roller positioned equidistant from the lower rollers over the thinnest part of the mid-  
195 diaphyseal region, to give an approximately posterior load direction. Femora were  
196 loaded at a crosshead speed of 2mm/min until failure, with load and displacement data  
197 recorded by a Zwick Z050 tensile testing machine fitted with a 1kN load cell (Zwick  
198 Testing Machines Ltd., Leominster, United Kingdom). Ultimate tensile stress was  
199 calculated using failure load, morphometric measurements of cortical wall thicknesses  
200 and diameter (taken from cross-sectional  $\mu$ -CT images corresponding to the fracture site  
201 as determined by measuring the distance from the end of the femur to the fracture point  
202 using a hand-held micrometer) and simple beam theory.

203

## 204 *Hormone Quantification*

205 Pituitaries were homogenized in 0.5ml lysis buffer (TRIS 0.1M pH 7.4, NaCl 0.15M,  
206 EGTA 1mM, EDTA 1mM, Triton 1%, Protease inhibitor cocktail (Sigma-Aldrich, P8340)  
207 and Phosphatase inhibitor cocktail 3 (Sigma- Aldrich, P0044)), maintained on ice for 30  
208 mins and centrifuged for 10 mins at 13000g. Protein concentration was measured in a  
209 1:100 dilution of 4 $\mu$ l of the supernatant with the QuantiPro BCA assay kit (Sigma Aldrich,  
210 QPBCA-1KT) using protein standards (Sigma-Aldrich, P0914). Samples were diluted in  
211 PBS to normalize protein concentration. GH, LH and PRL levels were measured using  
212 sandwich ELISAs ([Steyn et al, 2011](#); [Steyn et al, 2013](#), [Guillou et al, 2015](#)).

213

214 Plasma IGF-1 concentrations were determined in duplicate using a rat/mouse total IGF-1  
215 immunoenzymometric assay (OCTEIA® Immunodiagnostic Systems Ltd., #AC-18F1)  
216 according to the manufacturer's instructions, with samples pre-treated to avoid binding  
217 protein interference. LH and FSH levels were measured in plasma samples using  
218 radioimmunoassay reagents provided by the National Institutes of Health (Dr. A. F.  
219 Parlow, Torrance, CA, USA). Rat LH-I-10 and FSH-I-9 were labeled with <sup>125</sup>I by the  
220 chloramine-T method, and LH and FSH concentrations expressed using reference  
221 preparations LH-RP-3 and FSH-RP-2 as standards. Intra- and inter-assay coefficients of  
222 variation were <8% and <10% for LH and <6% and <9% for FSH, respectively. Assay  
223 sensitivities were 5 pg/tube for LH and 20 pg/tube for FSH.

224

## 225 *Statistical analyses*

226 Results are expressed as mean  $\pm$  SEM, and compared by unpaired Student's t-test or 1-  
227 way ANOVA and Bonferroni's selected pairs *post hoc* test (using GraphPad Prism,  
228 GraphPad Software Inc., San Diego. CA., USA), as indicated in the figure legends, with  
229  $P < 0.05$  considered significantly different.

## 230 **Results**

231

### 232 *Study 1. Tibial growth and marrow adiposity in PWS-IC<sup>del</sup> mice*

233 Tibial length and EPW were reduced in PWS-IC<sup>del</sup> males by 6% ( $P<0.001$ ; Fig 1A) and  
234 18% ( $P<0.01$ ; Fig 1B) respectively. A profound (79%) reduction in tibial marrow  
235 adiposity ( $P<0.05$ ; Fig 1C and inset pictures a & b) was due to a combination of a 53%  
236 reduction in marrow adipocyte number ( $P<0.05$ ; Fig 1D) and a 48% reduction in mean  
237 adipocyte size ( $P<0.05$ ; Fig 1E). Adipocyte size profiling (Fig 1F) revealed a loss of  
238 larger adipocytes, especially those  $>825\mu\text{m}^2$  ( $P<0.05$ ).

239

240 Analysis of TRAP<sup>+</sup>-stained sections revealed a 62% reduction in tibial osteoclast number  
241 ( $P<0.05$ ; data not shown), but when corrected for the 65% reduction in tibial trabecular  
242 surface ( $P<0.05$ ; data not shown), the osteoclast density was unaffected ( $P=0.403$ ; Fig  
243 1G).

244

### 245 *Study 2. Femoral phenotype in PWS-IC<sup>del</sup> mice*

246 A 4% reduction in femoral length in PWS-IC<sup>del</sup> mice ( $P<0.05$ ; Fig 2A) was accompanied  
247 by a 32% reduction in cortical (anterior-posterior) diameter ( $P<0.05$ ; Fig 2B) with mean  
248 cortical wall thickness in PWS-IC<sup>del</sup> mice being 73% of that in WT littermates ( $P=0.055$ ;  
249 Fig 2C).  $\mu\text{CT}$  analysis revealed that trabecular number (Tb.N) in the distal femora of  
250 PWS-IC<sup>del</sup> mice was reduced by 62% ( $P<0.01$ ; Fig 2D). Although the overall trabecular  
251 thickness (Tb.Th) was unaffected ( $P=0.110$ ; Fig 2E), the cross-sectional shape became  
252 more cylindrical (less plate-like) in PWS-IC<sup>del</sup> mice (structural modal index (SMI)  
253 increased by 25%;  $P<0.05$ ; Fig 2F). Trabecular surface was reduced in PWS-IC<sup>del</sup>  
254 femora by 72% ( $P=0.0006$ ; data not shown), but when corrected for the 77% reduction in  
255 trabecular volume ( $P=0.0009$ ; data not shown), relative trabecular surface (BS/BV) was

256 increased by 29% ( $P<0.01$ ; Fig 2G). These changes were accompanied by an 18%  
257 increase in trabecular separation (Tb.Sp;  $P<0.01$ ; Fig 2H) and a marked fragmentation of  
258 the trabecular lattice (63% increase in Pattern factor (Tb.Pf;  $P<0.05$ ; Fig 2I). Although  
259 mean degree of anisotropy in PWS-IC<sup>del</sup> mice was 125% of that in WT littermates, this  
260 index of trabecular orientation was not significantly different ( $P=0.098$ ; data not shown).

261

262 Biomechanical strength of PWS-IC<sup>del</sup> femoral cortex was reduced by 26% (ultimate  
263 moment;  $P<0.05$ ; Fig 3A). This was due to an 80% decrease in the geometric  
264 contribution to strength (second moment of area;  $P<0.05$ ; Fig 3C), the strength of the  
265 calcified tissue (ultimate tensile stress; UTS) being increased by 65% ( $P<0.05$ ; Fig 3B).

266

### 267 *Study 3. Endocrine status in PWS-IC<sup>del</sup> mice*

268 To investigate whether skeletal impairment might be due to endocrine dysfunction, we  
269 quantified pituitary and circulating hormone concentrations. Although not sexually  
270 dimorphic in either WT or PWS-IC<sup>del</sup> mice, pituitary weight was reduced in both male and  
271 female PWS-IC<sup>del</sup> mice by 35% and 43% respectively ( $P<0.01$  and  $P<0.001$ ; Fig 4A).  
272 Similarly, pituitary GH content was reduced by 42% and 56% in male and female PWS-  
273 IC<sup>del</sup> mice ( $P<0.05$ ; Fig 4B), in proportion to protein content (data not shown). While  
274 average pituitary PRL content in male PWS-IC<sup>del</sup> mice was only 45% of that in WT  
275 males, this was not significantly different ( $P>0.05$ ). In contrast, female PWS-IC<sup>del</sup> mice  
276 showed a 41% reduction in PRL content ( $P<0.05$ ; Fig 4C); the marked sexual  
277 dimorphism seen in WT mice ( $P<0.0001$ ) being retained in PWS-IC<sup>del</sup> littermates  
278 ( $P<0.01$ ; Fig 4C). This sexual dimorphism ( $P<0.0001$ ), but not PRL deficiency, was  
279 retained when PRL contents were corrected for protein content (data not shown). Male  
280 PWS-IC<sup>del</sup> mice showed a marked (58%) reduction in pituitary LH content ( $P<0.0001$ ; Fig  
281 4D), but while mean LH content in female PWS-IC<sup>del</sup> mice was only 54% of that in WT

282 females, this was not significantly different ( $P=0.535$ ; Fig 4D). In addition, the marked  
283 sexual dimorphism in LH content seen in WT mice ( $P<0.0001$ ) was not replicated in  
284 PWS-IC<sup>del</sup> littermates ( $P=0.412$ ). These differences in LH content remained after  
285 correction for protein content ( $P<0.05$ ; data not shown).

286

287 Circulating IGF-1 was reduced in male and female PWS-IC<sup>del</sup> mice by 47% and 37%  
288 respectively ( $P<0.0001$  and  $P<0.001$ ; Fig 5B). Although mean plasma LH and FSH  
289 concentration in PWS-IC<sup>del</sup> males were 163% and 123% of that in male WT littermates,  
290 these were not significantly different ( $P>0.900$ ; Fig 5C & D). Plasma LH and FSH  
291 concentrations were comparable in WT and PWS-IC<sup>del</sup> females and there was no sexual  
292 dimorphism in circulating gonadotrophin levels in either genotype (Fig 5C & D).

293

#### 294 *Study 4. The effect of thermoneutrality on skeletal parameters in PWS-IC<sup>del</sup> mice*

295 As in study 1, tibial length in male PWS-IC<sup>del</sup> mice at standard ambient temperature were  
296 reduced by 11% ( $P<0.0001$ ; Fig 6A), with a similar (10%) reduction in females  
297 ( $P<0.0001$ ; data not shown). This difference was maintained at thermoneutrality in  
298 males (9% reduction;  $P<0.001$ ; Fig 6A) and females (8% reduction;  $P<0.0001$ ),  
299 thermoneutrality having no effect on either tibial length nor EPW in either genotype (Fig  
300 6A & B).

301

302 Mean tibial marrow adiposity and adipocyte number in PWS-IC<sup>del</sup> mice at standard  
303 ambient temperature were only 22% and 29% of that in WT males, but given the  
304 variation in the WT data, these were not statistically different ( $P=0.5668$  (adiposity); Fig  
305 6C;  $P=0.3388$  (adipocyte number); Fig 6D). Thermoneutrality had no statistically  
306 significant effect on tibial marrow adiposity (Fig 6C) or adipocyte size in either WT or  
307 PWS-IC<sup>del</sup> males (Fig 6E). Parallel results were also obtained in females (data not

308 shown). Analysis of the adipocyte size profile revealed that while differences were seen  
309 between PWS-IC<sup>del</sup> males and their WT littermates at room temperature (e.g. there were  
310 less adipocytes in the size range 525-572 $\mu\text{m}^2$  in PWS-IC<sup>del</sup> mice (Fig 6F;  $P=0.038$ )),  
311 these differences were abolished in mice maintained at thermoneutrality (Fig 6G).

312

313 As above, femoral length and cortical diameter were reduced by 8% and 25% in male  
314 PWS-IC<sup>del</sup> mice at 20-22°C ( $P<0.0001$ ; Fig 7A & B), with average cortical wall thickness  
315 not being significantly different (Fig 7C). None of these geometric variables were altered  
316 by increasing the ambient temperature to thermoneutrality (Fig 7A-C). However, the  
317 48% reduction in the biomechanical strength of the femoral cortex in PWS-IC<sup>del</sup> mice at  
318 room temperature ( $P<0.0001$ ; Fig 7D), was abolished when PWS-IC<sup>del</sup> mice were  
319 maintained at thermoneutrality (Fig 7D). This improvement in biomechanical  
320 performance was entirely due to the significant increase in the strength of the calcified  
321 tissue, UTS in PWS-IC<sup>del</sup> mice at 30°C being 91% higher than in WT littermates at  
322 thermoneutrality ( $P<0.01$ ; Fig 7E). In the absence of any significant effect of  
323 thermoneutrality on femoral geometry, there was no change in the geometric contribution  
324 to strength, which remained at 32% of that in WT mice (Fig 7F). Similar results were  
325 obtained in females, the impaired biomechanical strength in PWS-IC<sup>del</sup> mice at 20-22°C  
326 ( $P=0.007$ ), being ameliorated at thermoneutrality ( $P=0.215$ ), as a consequence of the  
327 contribution of tissue strength, the impaired geometric contribution being exacerbated  
328 ( $P=0.006$ ) (data not shown).

329

## 330 Discussion

331 Loss of gene expression from the paternal allele of chromosome 15q11-q13 results in  
332 the marked disturbances in neural development, hormone secretion and metabolic  
333 homeostasis that characterise PWS. However, despite impaired GH secretion and GH  
334 replacement long being considered a key feature of this condition and an important  
335 element in therapeutic strategy (Lee et al, 1987; Deal et al, 2013; Carias & Wevrick,  
336 2019), our understanding of the significance of GH-deficiency for skeletal growth and  
337 integrity in the preclinical animal models of PWS is surprisingly superficial. To address  
338 this gap in our knowledge, we have analysed the phenotype of the weight-bearing long  
339 bones of the PWS-IC<sup>del</sup> mouse model for “full” PWS, shedding new light on the  
340 mechanisms of fracture risk in this complex condition.

341

342 Three prominent features of the observed skeletal phenotype deserve comment:  
343 impaired morphometric growth, impaired marrow adiposity and impaired biomechanical  
344 strength.

345

346 Preliminary evidence of growth retardation has been reported in most of the murine  
347 models for PWS, including mice with uniparental disomy (Cattanach et al, 1992) and  
348 deletions of *Snrpn-Ube3a* (Tsai et al, 1999a), *Snurf/Snrpn exon 2* (Tsai et al, 1999b),  
349 *Snord116* (Ding et al, 2008) and *Magel2* (Bischof et al, 2007; Baraghithy, 2019), with  
350 *Necdin<sup>del</sup>* mice showing normal growth (Tsai et al, 1999a). However, initial attempts to  
351 quantify skeletal growth following IC deletion, in which expression of all the genes in the  
352 PWS locus is lost, have been hampered by high neonatal mortality (Yang et al, 1998).  
353 Having developed a breeding strategy to partially overcome this problem, we now report  
354 that PWS-IC<sup>del</sup> mice display consistent shortening of appendicular bones.

355

356 This growth impairment is most likely to result from the marked deficiency in the GH-IGF-  
357 1 axis (40-50% reductions in both pituitary GH content and circulating IGF-1). Although  
358 we cannot exclude a potential reduction in GH sensitivity, it is evident from comparison  
359 with other murine models for isolated GH-deficiency (GH-D) or reduced GH signalling  
360 that the degree of growth retardation in mice appears to reflect the severity of axis  
361 inactivation, with complete loss of GH secretion/signalling producing the most severe  
362 phenotype (20-25% reduction in body length; [Alba and Salvatori, 2004](#); [Zhou et al, 1997](#);  
363 [Stevenson et al, 2009](#)).

364

365 It is important to note, however, that femoral diameter (reduced by 32% in PWS-IC<sup>del</sup>  
366 mice) was more profoundly affected than longitudinal growth. This occurred without  
367 affecting cortical wall thickness. Although broadly similar findings in mice with reduced  
368 GH signalling ([Stevenson et al, 2009](#)) suggest that loss of GH activity may be an  
369 important determinant, the fact that cortical diameter is only reduced by 17% in the  
370 complete absence of GH-receptors implies that other factors in the PWS endotype may  
371 contribute to this diminution of diameter.

372

373 While GH-deficiency may be the most likely cause, we cannot exclude the potentially  
374 negative influence of gonadotropin deficiency on bone formation ([Yarram et al, 2003](#)). In  
375 contrast, the observed PRL-deficiency is unlikely to represent a significant factor in this  
376 context as PRL has been shown to inhibit osteoblast function ([Cross et al, 2000](#)).

377 However, given the growing evidence for impaired oxytocin signalling in mouse models  
378 for PWS ([Schaller et al, 2010](#)), further analysis should investigate the potentially  
379 negative impact of oxytocin loss on the skeletal phenotype ([Elabd et al, 2008](#)).

380

381 A potential physical mechanism relates to the marked reduction in body weight (reduced  
382 by 40%) and adiposity (individual fat pad weights reduced by 67-84%) seen in PWS-IC<sup>del</sup>  
383 mice (Golding *et al*, 2017). This leanness has a number of consequences. Firstly, the  
384 loading forces being applied to these weight bearing bones are significantly reduced.  
385 These forces promote the remodelling of the bone to enhance diameter and weight-  
386 bearing capacity (David *et al*, 2007; Luu *et al*, 2009). Although muscle mass was not  
387 quantified in the current study, muscle hypoplasia in the *Mage12<sup>del</sup>* mouse model for  
388 PWS/Schaaf-Yang syndrome (SYS) (Kamaludin *et al*, 2016), indicates that this could  
389 represent a possible transduction mechanism. Secondly, such profound reductions in  
390 abdominal fat mass are likely to cause a dramatic reduction in circulating leptin. Any  
391 effect of hypoleptinaemia is likely to be enhanced by changes in the marrow milieu  
392 resulting from the equally dramatic reduction in marrow adiposity in this model.

393

394 This marked decline in tibial marrow adiposity is due to reductions in both marrow  
395 adipocyte number and size. While the latter parallels the changes we previously  
396 reported in intra-abdominal white adipose tissue (Golding *et al*, 2017), our current data  
397 indicates that in the bone marrow at least, impaired adipogenesis is also a significant  
398 factor. In the context of the barrage of endocrine signals promoting marrow adiposity,  
399 this is quite remarkable. For example, *dw/dw* rats, which show a similar degree of GH-D  
400 accompanied by intra-abdominal leanness, show elevated marrow adiposity (mainly  
401 increased adipogenesis) (Gevers *et al*, 2002), with GH treatment inhibiting adipogenesis  
402 and triglyceride storage (Gevers *et al*, 2002). In addition, since ghrelin is powerfully  
403 adipogenic in bone marrow (Thompson *et al*, 2004; Davies *et al*, 2009; Hopkins *et al*,  
404 2017), the marked hyperghrelinaemia in PWS-IC<sup>del</sup> mice (Golding *et al*, 2017) should  
405 elevate marrow adiposity. Clearly, the anti-adipogenic signals in PWS-IC<sup>del</sup> mice are  
406 more than sufficient to reverse these influences. The absence of the larger adipocytes in

407 bone marrow corresponds with the reported impairment of lipid storage capacity in intra-  
408 abdominal WAT in these mice (Golding *et al*, 2017) and the impairment of lipid storage in  
409 cultured adipocytes from humans with PWS (Cadoudal *et al*, 2014). Whether the obesity  
410 that usually accompanies PWS in humans leads to parallel changes in marrow adiposity  
411 remains to be established.

412

413 With this degree of leanness in the marrow, it is highly likely that the production of leptin  
414 from marrow adipocytes (Laharrague *et al*, 1998) is reduced in parallel. Interestingly,  
415 intra-bone marrow infusion of leptin in GH-D rats not only halves marrow adiposity by  
416 suppressing adipogenesis, but increases osteoblast surface (Evans *et al*, 2011). Given  
417 this role of leptin in maintaining the bone microenvironment, one would expect bones  
418 from PWS-IC<sup>del</sup> mice to show evidence of elevated osteoblast activity. However, while  
419 the function of PWS-IC<sup>del</sup> osteoblasts should be examined *in vitro*, our data indicate that  
420 osteoblast activity does not appear to be enhanced *in vivo*. Indeed, the combination of  
421 unaltered relative trabecular surface, a more fragmented trabecular lattice and an  
422 unchanged osteoclast density, imply that PWS-IC<sup>del</sup> osteoblast number and/or activity is  
423 reduced. The combined reduction in adipocytes and osteoblasts is unusual and  
424 suggests a failure in the proliferation of MSCs or their subsequent differentiation.

425

426 In the context of this endocrine and cellular milieu, the biomechanical integrity of the  
427 femoral cortex is clearly compromised. Surprisingly, UTS, a measure of the strength of  
428 the calcified tissue, *per se*, is significantly increased. Such increases in tissue strength  
429 usually result from a greater density of either matrix proteins or hydroxyapatite. This is  
430 likely to be due to the reduction in GH-axis activity, producing slower growing and less  
431 remodelled bone (Locatelli & Bianchi, 2014). Nevertheless, despite this increased tissue  
432 strength, the geometric component of strength (second moment of area) is profoundly

433 reduced, which corresponds directly with the smaller cortical diameter discussed above.  
434 Indeed, the impairment of this geometric component is more than sufficient to translate  
435 an elevated UTS into a compromised overall organ strength.

436

437 While the analysis of single-gene deletion models in this context is far from complete, the  
438 information available suggests some potential genetic mechanisms underlying the  
439 complex skeletal phenotype observed. The impairment of the GH-axis may be due in  
440 part to the loss of expression of *Snord116*, because although *Snord116<sup>del</sup>* mice show  
441 normal pituitary volume, somatotroph number (Ding *et al*, 2008) and GH content (Burnett  
442 *et al*, 2017), circulating IGF-1 is reduced by 60-70% (Ding *et al*, 2008; Qi *et al*, 2016).  
443 This lack of GH action, possibly as the result of impaired activity of the hormone pro-  
444 convertase enzyme PC1 (Burnett *et al*, 2017) increases GH-releasing hormone mRNA  
445 expression in the arcuate nucleus (Qi *et al*, 2016) reflecting impaired GH feedback. In  
446 contrast, male *Mage12<sup>del</sup>* mice show normal IGF-1 levels, with IGF-1 secretion and  
447 ghrelin-induced (but not GHRH-induced) GH responses impaired in female mice  
448 (Tennese & Wevrick, 2011). However, given the episodic nature of GH secretion in  
449 rodents, establishing the relationship between these specific genes and the parameters  
450 of spontaneous GH secretion would be more readily achieved in a larger species.

451

452 In the context of skeletal growth, body length is only modestly reduced in *Snord116<sup>del</sup>*  
453 mice, with a 10% reduction in bone mineral density (Ding *et al*, 2008; Qi *et al*, 2016).  
454 Although overall body length is normal in the absence of *Mage12* (Bischof *et al*, 2007),  
455 femoral length, cortical diameter and cortical wall thickness are reduced in female  
456 *Mage12<sup>del</sup>* mice by 9-13% (Baraghithy *et al*, 2019). Indeed, this is the only model in which  
457 a comprehensive analysis has been made of the skeletal phenotype. Interestingly,  
458 although these mice also show comparable reductions in trabecular number, trabecular

459 fragmentation, femoral strength and UTS to that reported here in the PWS-IC<sup>del</sup> mice,  
460 marrow adiposity is more than doubled ([Baraghithy et al, 2019](#)) compared to the  
461 profound reduction reported here. This implies that loss of one of the other genes in the  
462 PWS locus either disrupts the relationship between adipocyte and osteoblast  
463 differentiation, or the proliferation of MSCs. Since *Necdin* has already been identified as  
464 a regulator of astrocyte ([Fujimoto et al, 2016](#)), neocortical neural precursor cell  
465 ([Minamide et al, 2014](#)), hematopoietic stem cell ([Asai et al, 2012](#)) and pre-adipocyte  
466 ([Fujiwara et al, 2012](#)) differentiation, this seems like a potential candidate.

467

468 Given that the normal relationship between fat mass and bone remodelling is disrupted  
469 in PWS-IC<sup>del</sup> mice, and our previous evidence that raising ambient temperature  
470 suppresses brown adipose tissue function ([Golding et al, 2017](#)), we investigated the  
471 effects of maintaining PWS-IC<sup>del</sup> mice at thermoneutrality on this altered skeletal  
472 phenotype. While this manipulation had no effect on marrow adiposity, there was a  
473 significant improvement in biomechanical strength as a result of an increased strength of  
474 the calcified tissue. This is remarkable since we have previously shown that this  
475 manipulation halved food intake in PWS-IC<sup>del</sup> mice ([Golding et al, 2017](#)). When coupled  
476 with evidence that thermoneutrality normalises skeletal length and bone mineral density  
477 in *Snord116<sup>del</sup>* mice ([Qi et al, 2017](#)), this implies that bone turnover is dramatically  
478 reduced at thermoneutrality. This interpretation is supported by evidence that  
479 thermoneutrality increases bone formation and reduces bone resorption in growing  
480 female C17BL/6J mice, while dramatically reducing food intake and doubling marrow  
481 adiposity ([Iwaniec et al, 2016](#)). The latter observation serves to re-emphasize the likely  
482 impairment of adipocyte function in the PWS-IC<sup>del</sup> model ([Golding et al, 2017](#)).

483

484 In summary, our data show that the longitudinal growth and biomechanical integrity of  
485 long bones are markedly impaired in the PWS-IC<sup>del</sup> mouse model for “full” PWS.  
486 Whether this impairment is matched by deficits in the biomechanical properties of other  
487 types of bone, e.g. calvarial or vertebral bone, has yet to be established, but our data not  
488 only provide a biomechanical basis for the increased fracture risk in PWS ([Butler \*et al\*, 2002](#);  
489 [Longhi \*et al\*, 2015](#)), but indicate that thermoneutrality may be beneficial in this  
490 context. The final phenotype observed in the PWS-IC<sup>del</sup> mice appears to result from the  
491 combined loss of several genes from within the PWS locus, but a more precise genetic  
492 cause for the individual aspects remains to be fully elucidated.

493 **References**

- 494 Alba M & Salvatori R 2004 A mouse with targeted ablation of the growth hormone-  
495 releasing hormone gene: a new model of isolated growth hormone deficiency.  
496 *Endocrinology* **145** 4134-4143. (doi: <https://doi.org/10.1210/en.2004-0119>)  
497
- 498 Asai T, Liu Y, Di Giandomenico S, Bae N, Ndiaye-Lobry D, Deblasio A, Menendez S,  
499 Antipin Y, Reva B, Wevrick R *et al* 2012 Necdin, a P53 target gene, regulates the  
500 quiescence and response to genotoxic stress in hematopoietic stem/progenitor cells.  
501 *Blood* **120** 1601-1612. (doi: [10.1182/blood-2011-11-393983](https://doi.org/10.1182/blood-2011-11-393983))  
502
- 503 Baraghithy S, Smoum R, Drori A, Hdar R, Gammal, A, Hirsch S, Attar-Namdar M,  
504 Nemirovski A, Gabet Y, Langer Y *et al* 2019 *Mage12* modulates bone remodelling and  
505 mass in Prader-Willi syndrome by affecting oleoyl serine levels and activity. *Journal of*  
506 *Bone and Mineral Research* **34** 93-105 (doi: <https://doi.org/10.1002/jbmr.3591>)  
507
- 508 Beresford JN, Bennett JH, Devlin C, Leboy PS & Owen ME 1992 Evidence for an  
509 inverse relationship between the differentiation of adipocytic and osteogenic cells in rat  
510 marrow stromal cell cultures. *Journal of Cell Science* **102** 341-351. (PMID: [1400636](https://pubmed.ncbi.nlm.nih.gov/1400636/))  
511
- 512 Bischof JM, Stewart CL & Wevrick R 2007 Inactivation of the mouse *Mage12* gene  
513 results in growth abnormalities similar to Prader-Willi syndrome. *Human Molecular*  
514 *Genetics* **16** 2713-2719. (doi: [10.1093/hmg/ddm225](https://doi.org/10.1093/hmg/ddm225))  
515
- 516 Boussein ML, Boyd SK, Christiansen BA, Guldberg RE, Jepsen KJ & Müller R 2010  
517 Guidelines for assessment of bone microarchitecture in rodents using micro-computed  
518 tomography. *Journal of Bone and Mineral Research* **25** 1468-1486 (doi:  
519 [10.1002/jbmr.141](https://doi.org/10.1002/jbmr.141))  
520
- 521 Burnett LC, LeDuc CA, Sulsona CR, Paul D, Rausch R, Eddiry A, Martin Carli JF,  
522 Morabito MV, Skowronski AA, Hubner G *et al* 2017 Deficiency in prohormone  
523 convertase PC1 impairs prohormone processing in Prader-Willi syndrome. *Journal of*  
524 *Clinical Investigation* **127** 293-305. (doi: [10.1172/JCI88648](https://doi.org/10.1172/JCI88648))  
525
- 526 Butler JV, Whittington JE, Holland AJ, Boer H, Clarke D & Webb T 2002 Prevalence of,  
527 and risk factors for, physical ill-health in people with Prader-Willi syndrome: a population-  
528 based study. *Developmental Medicine and Child Neurology* **44** 248-255 (doi:  
529 <https://doi.org/10.1017/S001216220100202X>)  
530
- 531 Butler MG, Manzardo AM & Forster JL 2016 Prader-Willi syndrome: clinical genetics  
532 and diagnostic aspects with treatment approaches. *Current Pediatric Reviews* **12** 136-  
533 166. (doi: [10.2174/1573396312666151123115250](https://doi.org/10.2174/1573396312666151123115250))  
534
- 535 Cadoudal T, Buléon M, Segenès C, Diene G, Desneulin F, Molinas C, Eddiry S, Conte-  
536 Auriol F, Daviaud D, Martin PG *et al*. 2014 Impairment of adipose tissue in Prader-Willi  
537 syndrome rescued by growth hormone treatment. *International Journal of Obesity*  
538 *(London)* **38** 1234-1240. (doi: [10.1038/ijo.2014.3](https://doi.org/10.1038/ijo.2014.3))  
539
- 540 Carias KV & Wevrick R 2019 Preclinical testing in translational animal models of  
541 Prader-Willi syndrome: overview and gap analysis. *Molecular Therapy: Methods &*  
542 *Clinical Assessment* **13** 344-358. (doi: <https://doi.org/10.1016/j.omtm.2019.03.001>)

- 543  
544 Cattanach BM, Barr JA, Evans EP, Burtenshaw M, Beechey CV, Leff SE, Brannan CI,  
545 Copeland NG, Jenkins NA & Jones J 1992 A candidate mouse model for Prader-Willi  
546 syndrome which shows an absence of Snrpn expression. *Nature Genetics* **2** 270-274.  
547 (doi: [10.1038/ng1292-270](https://doi.org/10.1038/ng1292-270))  
548  
549 Chamberlain SJ, Johnstone KA, DuBose AJ, Simon TA, Bartolomei MS, Resnick JL &  
550 Brannan CI 2004 Evidence for genetic modifiers of postnatal lethality in PWS-IC  
551 deletion mice. *Human Molecular Genetics* **13** 2971-2977. (doi: [10.1093/hmg/ddh314](https://doi.org/10.1093/hmg/ddh314))  
552  
553 Cross D, Yang Y, Kuo CB, Xu X, Luben RA & Walker AM 2000 Effects of prolactin on  
554 osteoblast alkaline phosphatase and bone formation in the developing rat. *American*  
555 *Journal of Physiology Endocrinology and Metabolism* **279** E1216-E1226. (doi:  
556 [10.1152/ajpendo.2000.279.6.E1216](https://doi.org/10.1152/ajpendo.2000.279.6.E1216))  
557  
558 Cummings DE, Clement K, Purnell JQ, Vaisse C, Foster KE, Frayo RS, Schwartz MW,  
559 Basdevant A & Weigle DS 2002 Elevated plasma ghrelin levels in Prader-Willi  
560 syndrome. *Nature Medicine* **8** 643-644. (doi: [10.1038/nm0702-643](https://doi.org/10.1038/nm0702-643))  
561  
562 David V, Martin A, Lafage-Proust M-H, Malaval L, Peyroche S, Jones DB, Vico L &  
563 Guignandon A 2007 Mechanical loading down-regulates peroxisome proliferator-  
564 activated receptor  $\gamma$  in bone marrow stromal cells and favours osteoblastogenesis at the  
565 expense of adipogenesis. *Endocrinology* **148** 2553-2562. (doi: [10.1210/en.2006-1704](https://doi.org/10.1210/en.2006-1704))  
566  
567 Davies JS, Kotokorpi P, Eccles SR, Barnes SK, Tokarczuk PF, Allen SK, Whitworth HS,  
568 Guschina IA, Evans BA, Mode A *et al* 2009 Ghrelin induces abdominal obesity via  
569 GHS-R-dependent lipid retention. *Molecular Endocrinology* **23** 914-924. (doi:  
570 [10.1210/me.2008-0432](https://doi.org/10.1210/me.2008-0432))  
571  
572 Deal CL, Tony M, Höybye C, Allen DB, Tauber M, Christiansen JS, and the 2011 Growth  
573 Hormone in Prader-Willi Syndrome Clinical Care Guidelines Workshop Participants  
574 2013. Growth Hormone Research Society Workshop Summary: consensus guidelines  
575 for recombinant human growth hormone therapy in Prader-Willi syndrome. *Journal of*  
576 *Clinical Endocrinology and Metabolism* **98** E1072-E1087. (doi: [10.1210/jc.2012-3888](https://doi.org/10.1210/jc.2012-3888))  
577  
578 Di Iorgi, Rosol M, Mittelman SD & Gilsanz V 2008 Reciprocal relation between marrow  
579 adiposity and the amount of bone in the axial and appendicular skeleton of young adults.  
580 *Journal of Clinical Endocrinology and Metabolism* **93** 2281-2286. (doi: [10.1210/jc.2007-2691](https://doi.org/10.1210/jc.2007-2691))  
581  
582  
583 Ding F, Li HH, Zhang S, Solomon NM, Camper SA, Cohen P & Franke U 2008  
584 SnoRNA Snord116 (Pwcr/MBII-85) deletion causes growth deficiency and hyperphagia  
585 in mice. *PLoS One* **3** 31709. (doi: [10.1371/journal.pone.0001709](https://doi.org/10.1371/journal.pone.0001709)).  
586  
587 Elabd C, Basillais A, Beaupied H, Breuil V, Wagner N, Scheideler M, Zaragosi LE,  
588 Massiéra F, Lemichez E, Benhamou CL, Dani C, Amri EZ 2008 Oxytocin controls  
589 differentiation of human mesenchymal stem cells and reverses osteoporosis. *Stem Cells*  
590 **26** 2399-2407. (doi: [10.1634/stemcells.2008-0127](https://doi.org/10.1634/stemcells.2008-0127))  
591  
592 Evans BAJ, Bull MJ, Kench RC, Fox RE, Morgan LD, Stevenson AE, Gevers EF, Perry  
593 MJ & Wells T 2011 The influence of leptin on trabecular architecture and marrow

- 594 adiposity in GH-deficient rats. *Journal of Endocrinology* **208** 69-79. (doi: [10.1677/JOE-](https://doi.org/10.1677/JOE-10-0178)  
595 [10-0178](https://doi.org/10.1677/JOE-10-0178))  
596
- 597 Fujimoto I, Hasegawa K, Fujiwara K, Yamada M & Yoshikawa K 2016 Necdin controls  
598 EGFR signalling linked to astrocyte differentiation in primary cortical progenitor cells.  
599 *Cellular Signalling* **28** 94-017. (doi: [10.1016/j.cellsig.2015.11.016](https://doi.org/10.1016/j.cellsig.2015.11.016))  
600
- 601 Fujiwara K, Hasegawa K, Ohkumo T, Miyoshi H, Tseng YH & Yoshikawa K 2012 Necdin  
602 controls proliferation of white adipose progenitor cells. *PLoS One* **7** e30948. (doi:  
603 [10.1371/journal.pone.0030948](https://doi.org/10.1371/journal.pone.0030948))  
604
- 605 Gevers EF, Loveridge N & Robinson IC 2002 Bone marrow adipocytes: a neglected  
606 target tissue for growth hormone. *Endocrinology* **143** 4065-4073. (doi:  
607 [10.1210/en.2002-220428](https://doi.org/10.1210/en.2002-220428))  
608
- 609 Golding DM, Rees DJ, Davies JR, Relkovic D, Furby HV, Guschina IA, Davies JS,  
610 Resnick JL, Isles AR & Wells T. 2017. Paradoxical leanness in the imprinting-centre  
611 deletion mouse model for Prader-Willi syndrome. *Journal of Endocrinology* **232** 123-  
612 135. (doi: [10.1530/JOE-16-0367](https://doi.org/10.1530/JOE-16-0367))  
613
- 614 Grosso S, Cioni M, Peruzzi L, Pucci L & Berardi R 1998 Growth hormone secretion in  
615 Prader-Willi syndrome. *Journal of Endocrinological Investigation* **21** 418-422. (doi:  
616 [10.1007/BF03347319](https://doi.org/10.1007/BF03347319))  
617
- 618 Guillou A, Romanò N, Steyn F, Abitbol K, Le Tissier P, Bonnefont X, Chen C, Mollard P  
619 & Martin AO. 2015. Assessment of lactotroph axis functionality in mice: longitudinal  
620 monitoring of PRL secretion by ultrasensitive-ELISA. *Endocrinology* **156**:1924-30. (doi:  
621 [10.1210/en.2014-1571](https://doi.org/10.1210/en.2014-1571))  
622
- 623 Hamrick MW, Della-Fera MA, Choi Y-H, Pennington C, Hartzell D & Baile CA 2005  
624 Leptin treatment induces loss of bone marrow adipocytes and increases bone formation  
625 in leptin-deficient *ob/ob* mice. *Journal of Bone and Mineral Research* **20** 994-1001. (doi:  
626 [10.1359/JBMR.050103](https://doi.org/10.1359/JBMR.050103))  
627
- 628 Hopkins AL, Nelson TAS, Guschina IA, Parsons LC, Lewis CL, Brown RC, Christian HC,  
629 Davies JS & Wells T 2017 Unacylated ghrelin promotes adipogenesis in rodent bone  
630 marrow via ghrelin O-acyl transferase and GHS-R<sub>1a</sub> activity: evidence for target cell-  
631 mediated acylation. *Scientific Reports* **7** 45541. (doi: [10.1038/srep45541](https://doi.org/10.1038/srep45541))  
632
- 633 Iwaniec UT, Philbrick KA, Wong CP, Gordon JL, Kahler-Quesada AM, Olson DA,  
634 Brancum AJ, Sargent JL, DeMambro VE, Rosen CJ *et al.* 2016. Room temperature  
635 housing results in premature cancellous bone loss in growing female mice: implications  
636 for the mouse as a preclinical model for age-related bone loss. *Osteoporosis*  
637 *International* **27** 3091-3101 (doi: [10.1007/s00198-016-3634-3](https://doi.org/10.1007/s00198-016-3634-3))  
638
- 639 Kamaludin AA, Smolarchuk C, Bischof JM, Eggert R, Greer JJ, Ren J, Lee JJ, Yokota T,  
640 Berry FB & Wevrick R 2016 Muscle dysfunction caused by loss of Magel2 in a mouse  
641 model of Prader-Willi and Schaaf-Yang syndromes. *Human Molecular Genetics* **25**  
642 3798-3809. (doi: [10.1093/hmg/ddw225](https://doi.org/10.1093/hmg/ddw225))  
643

- 644 Kahn MJ, Gerasimidis K, Edwards CA & Shaikh MG 2018 Mechanisms of obesity in  
645 Prader-Willi syndrome. *Pediatric Obesity* **13** 3-13. (doi: [10.1111/ijpo.12177](https://doi.org/10.1111/ijpo.12177))  
646
- 647 Khor EC, Fanshawe B, Qi Y, Zolotukhin S, Kulkarni RN, Enriquez RF, Purtell L, Lee NJ,  
648 Wee NK, Croucher PI, Campbell L *et al.* 2016 Prader-Willi critical region, a non-  
649 translated, imprinted central regulator of bone mass: possible role in skeletal  
650 abnormalities on Prader-Willi syndrome. *PLoS One* **11** e0148155.  
651 ([10.1371/journal.pone.0148155](https://doi.org/10.1371/journal.pone.0148155))  
652
- 653 Laharrague P, Larrouy D, Fontanilles AM, Truel M, Campfield A, Tenenbaum R, Galitzky  
654 J, Corberand JX, Pénicaud L & Casteilla L 1998 High expression of leptin by human  
655 bone marrow adipocytes in primary culture. *FASEB Journal* **12** 747-752. (PMID:  
656 [9619453](https://pubmed.ncbi.nlm.nih.gov/9619453/))  
657
- 658 Lee PD, Wilson DM, Rountree L, Hintz RL & Rosenfeld RG. 1987. Linear growth  
659 response to exogenous growth hormone in Prader-Willi syndrome. *American Journal of*  
660 *Medical Genetics* **28** 865-871. (doi: [10.1002/ajmg.1320280411](https://doi.org/10.1002/ajmg.1320280411))  
661
- 662 Leiben L, Callewaert F & Bouillon R 2009 Bone and metabolism: a complex crosstalk.  
663 *Hormone Research* **71** (Suppl 1) 134-138. (doi: <https://doi.org/10.1159/000178056>)  
664
- 665 Locatelli V & Bianchi VE 2014 Effect of GH/IGF-1 on bone metabolism and  
666 osteoporosis. *International Journal of Endocrinology* **2014** 235060. (doi:  
667 [10.1155/2014/235060](https://doi.org/10.1155/2014/235060))  
668
- 669 Longhi S, Grugni G, Gatti D, Spinnozzi E, Sartorio A, Adami S, Fanolla A & Radetti G  
670 2015 Adults with Prader-Willi syndrome have weaker bones: effect of treatment with GH  
671 and sex steroids. *Calcified Tissue International* **96** 160-166. (doi: [10.1007/s00223-014-9949-1](https://doi.org/10.1007/s00223-014-9949-1))  
672
- 673
- 674 Luu YK, Capilla E, Rosen CJ, Gilsanz V, Pessin JE, Judex S & Rubin CT 2009  
675 Mechanical stimulation of mesenchymal stem cell proliferation and differentiation  
676 promotes osteogenesis while preventing dietary-induced obesity. *Journal of Bone and*  
677 *Mineral Research* **24** 50-61. (doi: [10.1359/JBMR.080817](https://doi.org/10.1359/JBMR.080817))  
678
- 679 Miller JL, Lynn CH, Driscoll DC, Goldstone AP, Gold JA, Kimonis V, Dykens E, Butler  
680 MG, Shuster JJ & Driscoll DJ. 2011. Nutritional phases in Prader-Willi syndrome. *Am J*  
681 *Med Genet Part A* **155** 1040-1049. (doi: [10.1002/ajmg.a.33951](https://doi.org/10.1002/ajmg.a.33951))  
682
- 683 Minamide R, Fujiwara K, Hasegawa K & Yoshikawa K 2014 Antagonistic interplay  
684 between neccin and Bmi1 controls proliferation of neural precursor cells in the  
685 embryonic mouse neocortex. *PLoS One* **9** e84460. (doi:  
686 [10.1371/journal.pone.0084460](https://doi.org/10.1371/journal.pone.0084460))  
687
- 688 Muscatelli F, Abrous DN, Massacrier A, Boccaccio I, Le Moal M, Cau P & Cremer H  
689 2000 Disruption of the mouse Necdin gene results in hypothalamic and behavioural  
690 alterations reminiscent of the human Prader-Willi syndrome. *Human Molecular Genetics*  
691 **9** 3101-3110. (doi: [doi.org/10.1093/hmg/9.20.3101](https://doi.org/10.1093/hmg/9.20.3101))  
692
- 693 Navein AE, Cooke EJ, Davies JR, Smith TG, Wells LHM, Ohazama A, Healy C, Sharpe  
694 PT, Evans SL, Evans BAJ *et al* 2016. Disrupted mitochondrial function in the Opa3<sup>L122P</sup>

- 695 mouse model for Costeff Syndrome impairs skeletal integrity. *Human Molecular*  
696 *Genetics* **25**:2404-2416. (doi: [10.1093/hmg/ddw107](https://doi.org/10.1093/hmg/ddw107))  
697
- 698 Pravdivyi I, Ballanyi K, Colmers WF & Wevrick R 2015 Progressive postnatal decline in  
699 leptin sensitivity of arcuate hypothalamic neurons in the Magel2-null mouse model of  
700 Prader-Willi syndrome. *Human Molecular Genetics* **24** 5276-4283. (doi:  
701 [10.1093/hmg/ddv159](https://doi.org/10.1093/hmg/ddv159))  
702
- 703 Qi Y, Purtell L, Fu M, Lee NJ, Aepler J, Zhang L, Loh K, Enriquez RF, Baldock PA,  
704 Zolotukhin S *et al* 2016 Snord116 is critical in the regulation of food intake and body  
705 weight. *Scientific Reports* **6** 18614. (doi: [10.1038/srep18614](https://doi.org/10.1038/srep18614))  
706
- 707 Qi Y, Purtell L, Fu M, Sengmany K, Loh K, Zhang L, Zolotukhin S, Sainsbury A,  
708 Campbell L & Herzog H. 2017. Ambient temperature modulates the effects of the  
709 Prader-Willi syndrome candidate gene Snord116 on energy homeostasis.  
710 *Neuropeptides* **61** 87-93. (doi: [10.1016/j.npep.2016.10.006](https://doi.org/10.1016/j.npep.2016.10.006))  
711
- 712 Schaller F, Watrin F, Sturny R, Massacrier A, Szepetowski P, Muscatelli F 2003 A  
713 single postnatal injection of oxytocin rescues the lethal feeding behaviour in mouse  
714 newborns deficient for the imprinted Magel2 gene. *Human Molecular Genetics* **19** 4895-  
715 4905. (doi: [10.1093/hmg/ddq424](https://doi.org/10.1093/hmg/ddq424))  
716
- 717 Stevenson AE, Evans BAJ, Gevers EF, McLeod RWJ, Perry MJ, El-Kasti MM,  
718 Coschigano KT, Kopchick JJ, Evans SL & Wells T. 2009. Does adiposity status  
719 influence femoral cortical strength in rodent models of growth hormone deficiency?  
720 *American Journal of Physiology Endocrinology and Metabolism* **296** E147-E156. (doi:  
721 [10.1152/ajpendo.90689.2008](https://doi.org/10.1152/ajpendo.90689.2008))  
722
- 723 Steyn FJ, Huang L, Ngo ST, Leong JW, Tan HY, Xie TY, Parlow AF, Veldhuis JD,  
724 Waters MJ & Chen C 2011. Development of a method for the determination of pulsatile  
725 growth hormone secretion in mice. *Endocrinology* **152** 3165-3171. (doi:  
726 [10.1210/en.2011-0253](https://doi.org/10.1210/en.2011-0253))  
727
- 728 Steyn FJ, Wan Y, Clarkson J, Veldhuis JD, Herbison AE & Chen C 2013. Development  
729 of a methodology for and assessment of pulsatile luteinizing hormone secretion in  
730 juvenile and adult male mice. *Endocrinology* **155** 4939-4945. (doi: [10.1210/en.2013-1502](https://doi.org/10.1210/en.2013-1502))  
731
- 732
- 733 Tennese AA, Wevrick R 2011 Impaired hypothalamic regulation of endocrine function  
734 and delayed counterregulatory response to hypoglycaemia in Magel2-null mice.  
735 *Endocrinology* **152** 967-978. (doi: [10.1210/en.2010-0709](https://doi.org/10.1210/en.2010-0709))  
736
- 737 Thomas T, Gori F, Khosla S, Jensen MD, Burguera B & Riggs BL 1999 Leptin acts on  
738 human marrow stromal cells to enhance differentiation to osteoblasts and to inhibit  
739 differentiation to adipocytes. *Endocrinology* **140** 1630-1638. (doi:  
740 <https://doi.org/10.1210/endo.140.4.6637>)  
741
- 742 Thompson NM, Gill DAS, Davies R, Loveridge N, Houston PA & Robinson ICAF, Wells T  
743 2004 Ghrelin and des-octanoyl ghrelin promote adipogenesis directly *in vivo* by a  
744 mechanism independent of the type 1a growth hormone secretagogue receptor.  
745 *Endocrinology* **145** 234-242. (doi: <https://doi.org/10.1210/en.2003-0899>)

- 746  
747 Tilston TW, Brown RD, Wateridge MJ, Arms-Williams B, Walker JJ, Sun Y & Wells T  
748 2019 A novel automated system yields reproducible temporal feeding patterns in  
749 laboratory rodents. *Journal of Nutrition* in press (doi: <https://doi.org/10.1093/jn/nxz116>)  
750
- 751 Tsai TF, Armstrong D & Beaudet AL 1999a Necdin-deficient mice do not show lethality  
752 or the obesity and infertility of Prader-Willi syndrome. *Nature Genetics* **22** 15-16. (doi:  
753 [10.1038/8722](https://doi.org/10.1038/8722))  
754
- 755 Tsai TF, Jiang YH, Bressler J, Armstrong D & Beaudet AL 1999b Paternal deletion from  
756 Snrpn to Ube3a in the mouse causes hypotonia, growth retardation and partial lethality  
757 and provides evidence for a gene contributing to Prader-Willi syndrome. *Human*  
758 *Molecular Genetics* **8** 1357-1364. (doi: <https://doi.org/10.1093/hmg/8.8.1357>)  
759
- 760 Yang T, Adamson TE, Resnick JL, Leff S, Wevrick R, Franke U, Jenkins NA, Copeland  
761 NG & Brannan CI 1998 A mouse model for Prader-Willi syndrome imprinting-centre  
762 mutations. *Nature Genetics* **19** 25-31. (doi: [10.1038/ng0598-25](https://doi.org/10.1038/ng0598-25))  
763
- 764 Yarram SJ, Perry MJ, Christopher TJ, Westby K, Brown NL, Lamminen T, Rulli SB,  
765 Zhang FP, Huhtaniemi I, Sandy JR et al 2003 Luteinizing hormone receptor knockout  
766 (LuRKO) mice and transgenic human chorionic gonadotropin (hCG)-overexpressing  
767 mice (hCG alpha $\beta$ +) have bone phenotypes. *Endocrinology* **144** 2555-2564. (doi:  
768 [10.1210/en.2003-0036](https://doi.org/10.1210/en.2003-0036))  
769
- 770 Zhou Y, Xu BC, Maheshwari HG, He L, Reed M, Lozykowski M, Okada S, Cataldo L,  
771 Coschigamo K, Wagner TE *et al* 1997 A mammalian model for Laron syndrome  
772 produced by targeted disruption of the mouse growth hormone receptor / binding protein  
773 gene (the Laron mouse). *Proceedings of the National Academy of Sciences (USA)* **94**  
774 13215-13220. (doi: [10.1073/pnas.94.24.13215](https://doi.org/10.1073/pnas.94.24.13215))  
775

776 **Declaration of Interest**

777 The authors declare that there is no conflict of interest that could be perceived as  
778 prejudicing the impartiality of the research reported.

779

780 **Acknowledgments**

781 The authors thank JBIOS staff and Derek Scarborough (Cardiff University) for excellent  
782 technical support.

783

784 **Funding**

785 This work was supported by a summer studentship awarded by the Foundation for  
786 Prader-Willi Research (to TMB, BEK and TW). AG and PM were supported by grants  
787 from the Agence Nationale de la Recherche (ANR-15-CE14-0012-01, ANR-18-C14-  
788 0017-01), Institut National de la Santé et de la Recherche Médicale, Centre National de  
789 la Recherche Scientifique, and Université de Montpellier.

790 **Figure Legends**

791 **Figure 1: PWS-IC<sup>del</sup> mice show impaired tibial growth and adiposity.** Quantification  
792 of tibial length (A), in 18-month old male WT (n=6) and PWS-IC<sup>del</sup> (n=6) littermate mice.  
793 Tibial epiphysial plate (EP) width (B) was quantified in Masson's Trichrome-stained  
794 sections and tibial marrow adiposity (C), marrow adipocyte number (D), size (E) and  
795 Size profile (F) quantified in digital images of Toluidene Blue-stained sections from WT  
796 (a) and PWS-IC<sup>del</sup> (b) littermates. Osteoclast density (G) was quantified in TRAP<sup>+</sup>-  
797 stained sections. Data shown are mean  $\pm$  SEM (n=6 for both genotypes), with statistical  
798 comparisons performed by Student's unpaired T-test (\* $P$ <0.05; \*\* $P$ <0.01; \*\*\* $P$ <0.001 vs  
799 WT littermates).

800

801 **Figure 2: PWS-IC<sup>del</sup> mice show impaired femoral morphology.** Measurement of  
802 femoral length (A), outer cortical (anterior-posterior) diameter (A-P  $\emptyset$ ; B) and average  
803 cortical wall thickness (C) in 18-month old male WT (n=6 (3 for B & C)) and PWS-IC<sup>del</sup>  
804 (n=6) littermate mice.  $\mu$ -CT was used to quantify the number (Tb.N; D), thickness  
805 (Tb.Th; E), cross-sectional shape (Structural modal (SM) index; F), relative surface  
806 (BS/BV; G), separation (Tb.Sp; H) and lattice fragmentation (Pattern factor; I) of  
807 trabeculae in the distal femora. Data shown are mean  $\pm$  SEM, with statistical  
808 comparisons performed by Student's unpaired T-test (\* $P$ <0.05; \*\* $P$ <0.01 vs WT  
809 littermates).

810

811 **Figure 3: PWS-IC<sup>del</sup> mice show compromised femoral strength.** Measurement of  
812 femoral strength (Ultimate moment; A), tissue strength (Ultimate tensile stress; B) and  
813 the geometric contribution to strength (Second moment of area; C) in 18-month old male  
814 WT (n=6 (3 for B & C)) and PWS-IC<sup>del</sup> (n=6) littermate mice. Data shown are mean  $\pm$

815 SEM, with statistical comparisons performed by Student's unpaired T-test ( $*P<0.05$  vs  
816 WT littermates).

817

818 **Figure 4: PWS-IC<sup>del</sup> mice show multiple pituitary hormone deficiencies.**

819 Quantification of weight (A) and growth hormone (GH; B), prolactin (PRL; C) and  
820 luteinising hormone (LH; D) contents in 6-15-month old male and female WT (n=6) and  
821 PWS-IC<sup>del</sup> (n=6 (male) and 5 (female)) littermate mice. Data shown are mean  $\pm$  SEM,  
822 with statistical comparisons performed by 1-way ANOVA and Bonferroni post hoc test  
823 ( $*P<0.05$ ;  $**P<0.01$ ;  $***P<0.001$ ;  $****P<0.0001$  vs WT littermates (same sex);  $\dagger\dagger P<0.01$ ;  
824  $\dagger\dagger\dagger P<0.0001$  vs male littermates (same genotype)).

825

826 **Figure 5: PWS-IC<sup>del</sup> mice show reduced GH-IGF-1 axis activity.** Quantification of  
827 pituitary weight (A) and plasma insulin-like growth factor-1 (IGF-1; B), luteinising  
828 hormone (LH; C) and follicle stimulating hormone (FSH; D) in 5-9-month old male and  
829 female WT and PWS-IC<sup>del</sup> (n=6 per group) littermate mice. Data shown are mean  $\pm$   
830 SEM, with statistical comparisons performed by 1-way ANOVA and Bonferroni post hoc  
831 test (A & B) or Kruskal-Wallis test (C & D) ( $***P<0.001$ ;  $****P<0.0001$  vs WT littermates  
832 (same sex);  $\dagger\dagger\dagger P<0.0001$  vs male littermates (same genotype)).

833

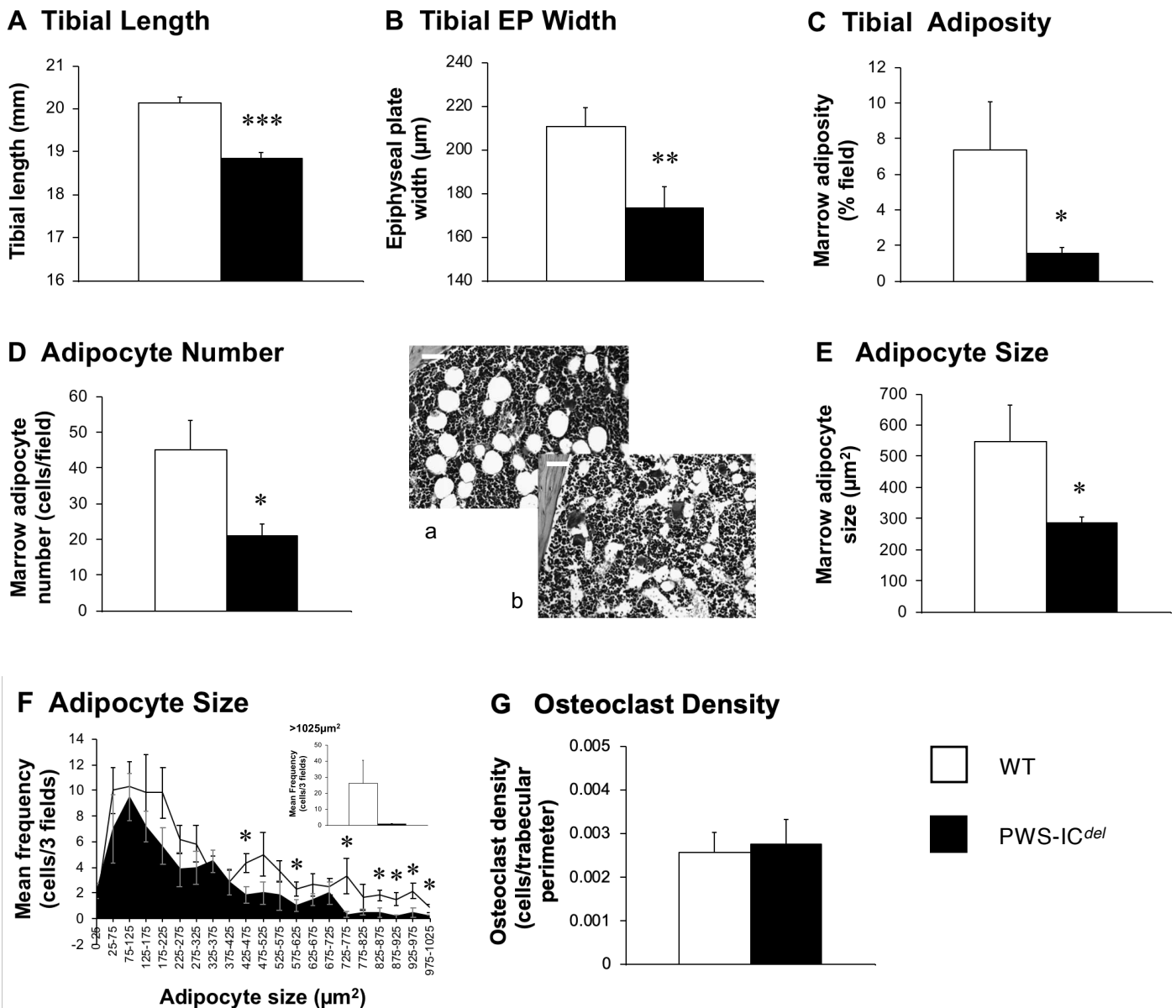
834 **Figure 6: Thermoneutrality has little effect on growth and marrow adiposity in**  
835 **PWS-IC<sup>del</sup> mice.** Tibial length (A), epiphyseal plate (EP) width (B), marrow adiposity (C),  
836 marrow adipocyte number (D) and mean adipocyte size (E) were quantified in 6-15-  
837 month old male WT and PWS-IC<sup>del</sup> after being maintained at either standard ambient  
838 temperature (20-22°C) or thermoneutrality (30°C) for 9 weeks. Adipocyte size profiles  
839 are presented for standard ambient temperature (F) and thermoneutrality (G). Data  
840 shown are mean  $\pm$  SEM (n=6 (room temperature) and 5 (thermoneutrality)), with

841 statistical comparisons performed by 1-way ANOVA and Bonferroni post hoc test (A-E;  
842 \*\*\*\*  $P < 0.0001$  vs room temperature (same genotype)) or unpaired Student's t-test (F &  
843 G; \*  $P < 0.05$  vs WT littermates (same temperature)).

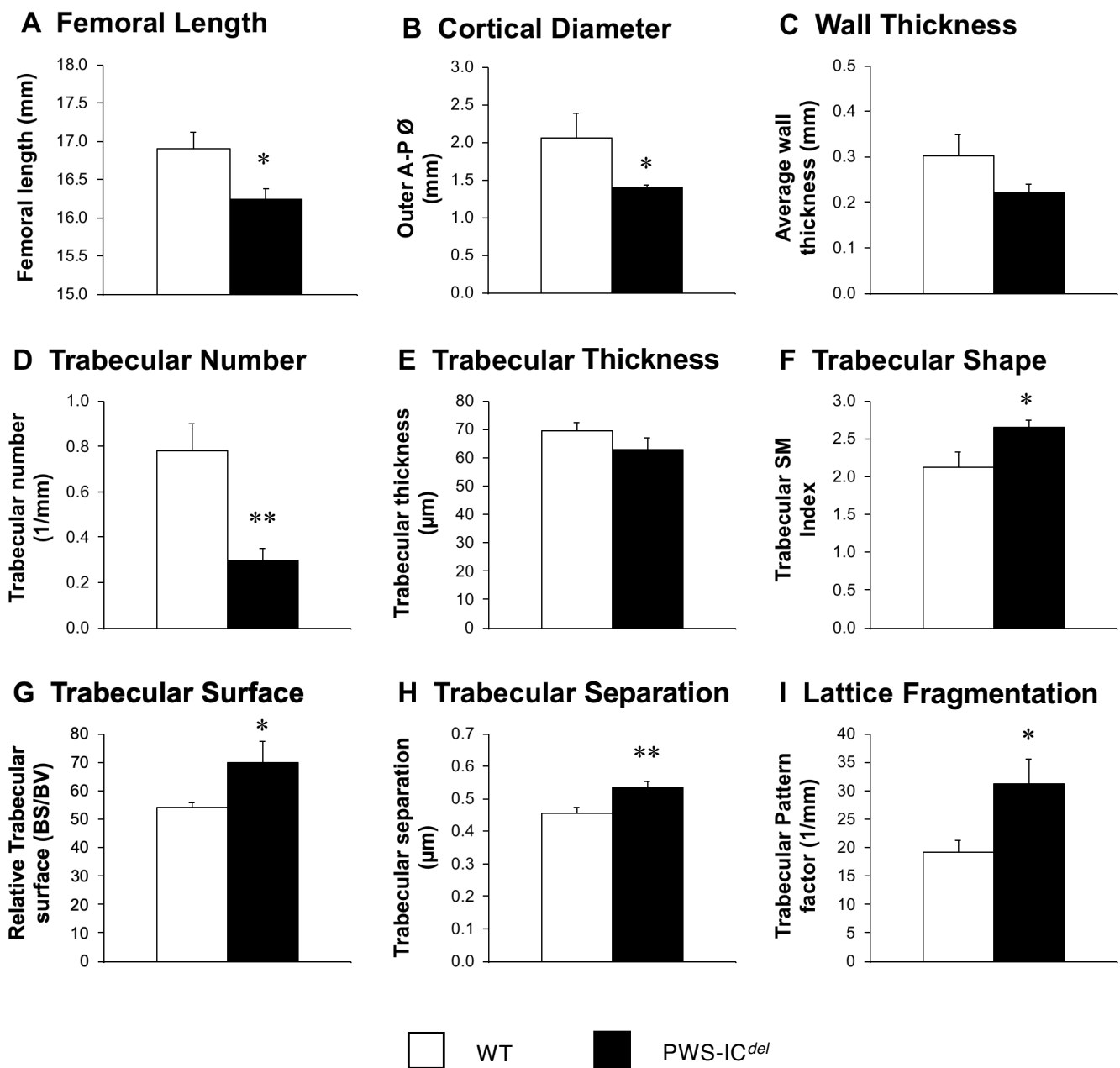
844

845 **Figure 7: Thermoneutrality has little effect on growth and marrow adiposity in**  
846 **PWS-IC<sup>del</sup> mice.** Tibial length (A), epiphyseal plate (EP) width (B), marrow adiposity (C),  
847 marrow adipocyte number (D) and mean adipocyte size (E) were quantified in 6-15-  
848 month old male WT and PWS-IC<sup>del</sup> after being maintained at either standard ambient  
849 temperature (20-22°C) or thermoneutrality (30°C) for 9 weeks (n=6 (room temperature)  
850 and 5 (thermoneutrality)). Data shown are mean  $\pm$  SEM, with statistical comparisons  
851 performed by 1-way ANOVA and Bonferroni post hoc test (\*\* $P < 0.01$ ; \*\*\*\* $P < 0.0001$  vs  
852 WT littermates (same ambient temperature)).

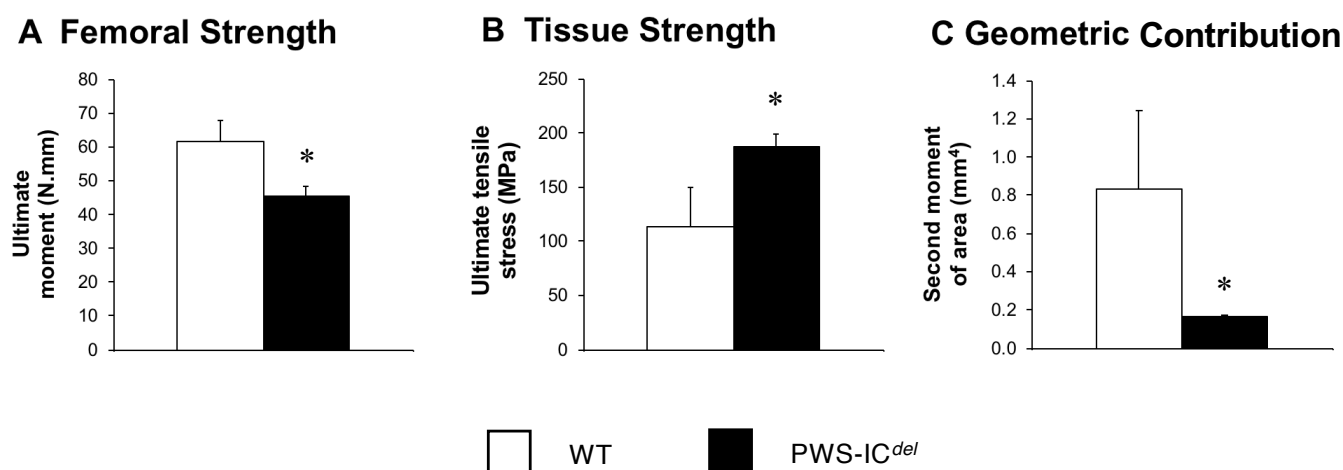
853



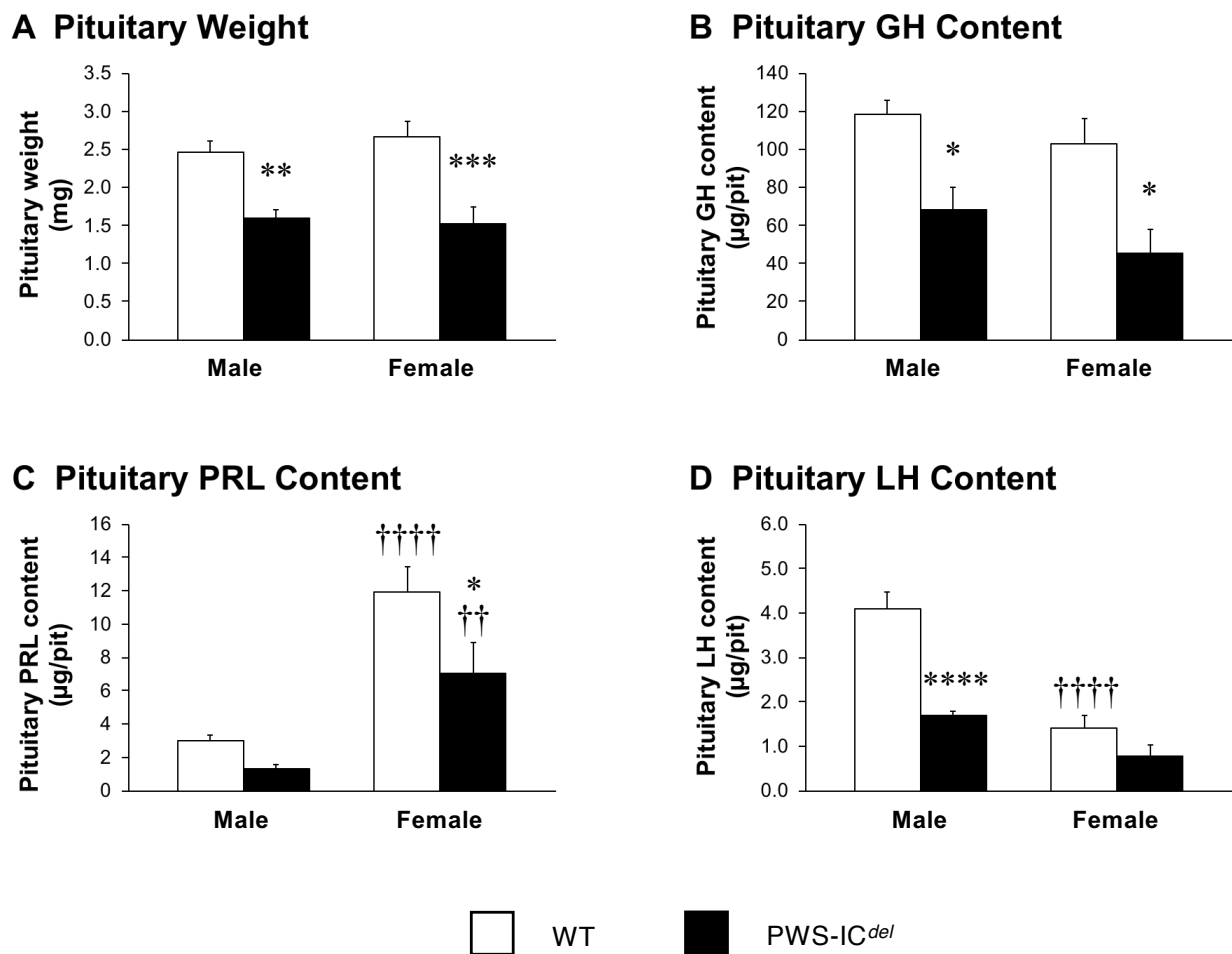
**Figure 1: PWS-IC<sup>del</sup> mice show impaired tibial growth and adiposity.** Quantification of tibial length (A), in 18-month old male WT (n=6) and PWS-IC<sup>del</sup> (n=6) littermate mice. Tibial epiphysal plate (EP) width (B) was quantified in Masson's Trichrome-stained sections and tibial marrow adiposity (C), adipocyte number (D), size (E) and Size profile (F) quantified in digital images of Toluidene Blue-stained sections from WT (a) and PWS-IC<sup>del</sup> (b) littermates. Osteoclast density (G) was quantified in TRAP<sup>+</sup>-stained sections. Data shown are mean ± SEM (n=6 for both genotypes), with statistical comparisons performed by Student's unpaired T-test (\**P*<0.05; \*\**P*<0.01; \*\*\**P*<0.001 vs WT littermates).



**Figure 2: PWS-IC<sup>del</sup> mice show impaired femoral morphology.** Measurement of femoral length (A), outer cortical (anterior-posterior) diameter (A-P Ø; B) and average cortical wall thickness (C) in 18-month old male WT (n=6 (3 for B & C)) and PWS-IC<sup>del</sup> (n=6) littermate mice.  $\mu$ -CT was used to quantify the number (Tb.N; D), thickness (Tb.Th; E), cross-sectional shape (Structural modal (SM) index; F), relative surface (BS/BV; G), separation (Tb.Sp; H) and lattice fragmentation (Pattern factor; I) of trabeculae in the distal femora. Data shown are mean  $\pm$  SEM, with statistical comparisons performed by Student's unpaired T-test (\* $P < 0.05$ ; \*\* $P < 0.01$  vs WT littermates).



**Figure 3: PWS-IC<sup>del</sup> mice show compromised femoral strength.** Measurement of femoral strength (Ultimate moment; A), tissue strength (Ultimate tensile stress; B) and the geometric contribution to strength (Second moment of area; C) in 18-month old male WT (n=6 (3 for B & C)) and PWS-IC<sup>del</sup> (n=6) littermate mice. Data shown are mean ± SEM, with statistical comparisons performed by Student's unpaired T-test (\*P<0.05 vs WT littermates).

Braxton TM *et al*, 2019; Figure 4**Figure 4: PWS-IC<sup>del</sup> mice show multiple pituitary hormone deficiencies.**

Quantification of weight (A) and growth hormone (GH; B), prolactin (PRL; C) and luteinising hormone (LH; D) contents in 6-15-month old male and female WT (n=6) and PWS-IC<sup>del</sup> (n=6 (male) and 5 (female)) littermate mice. Data shown are mean  $\pm$  SEM, with statistical comparisons performed by 1-way ANOVA and Bonferroni post hoc test (\* $P$ <0.05; \*\* $P$ <0.01; \*\*\* $P$ <0.001; \*\*\*\* $P$ <0.0001 vs WT littermates (same sex); †† $P$ <0.01; ††††  $P$ <0.0001 vs male littermates (same genotype)).

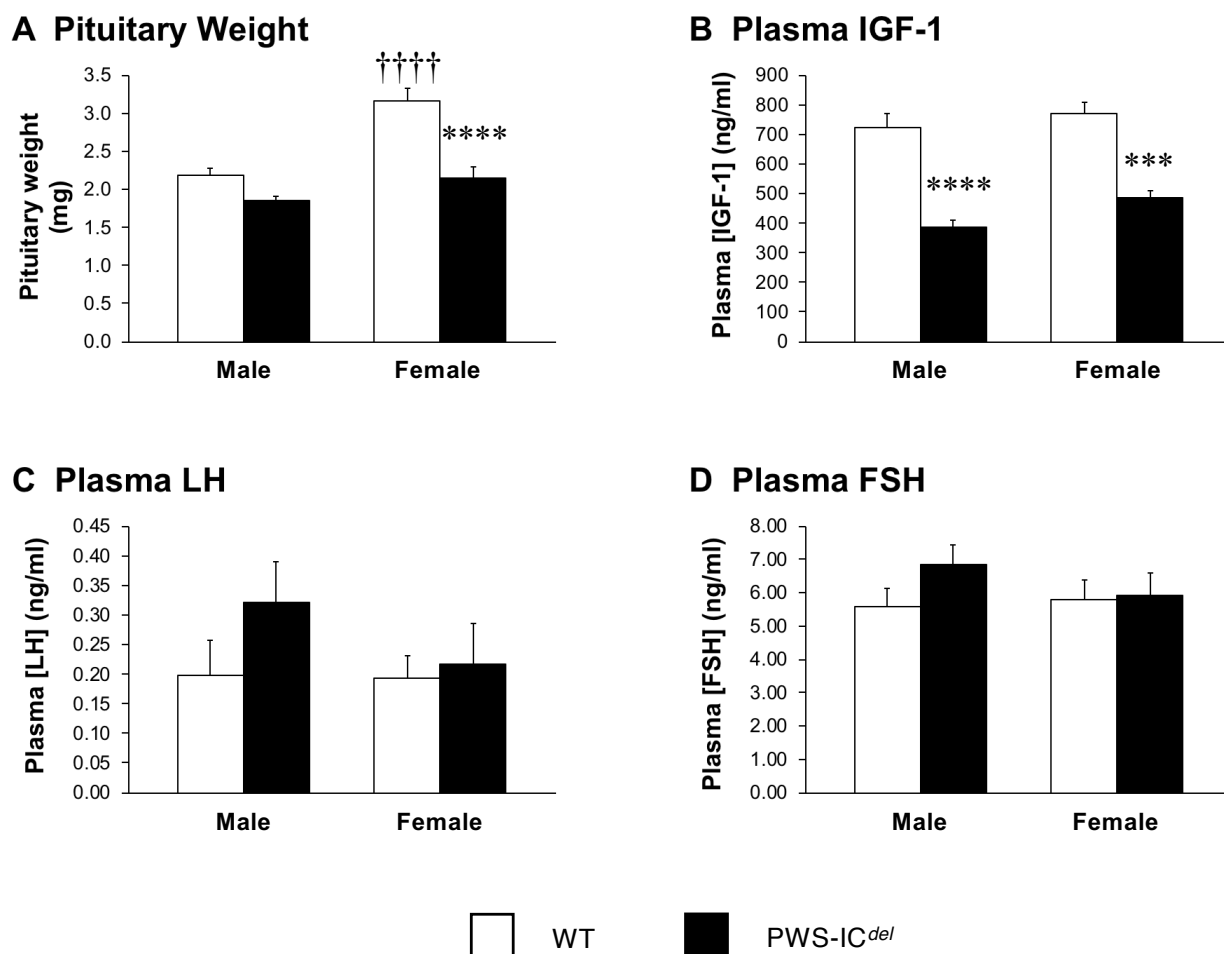


**Figure 5: PWS-IC<sup>del</sup> mice show reduced GH-IGF-1 axis activity.** Quantification of pituitary weight (A) and plasma insulin-like growth factor-1 (IGF-1; B), luteinising hormone (LH; C) and follicle stimulating hormone (FSH; D) in 5-9-month old male and female WT and PWS-IC<sup>del</sup> (n=6 per group) littermate mice. Data shown are mean  $\pm$  SEM, with statistical comparisons performed by 1-way ANOVA and Bonferroni post hoc test (A & B) or Kruskal-Wallis test (C & D) (\*\* $P$ <0.001; \*\*\*\* $P$ <0.0001 vs WT littermates (same sex); ††††  $P$ <0.0001 vs male littermates (same genotype)).

## Braxton TM et al, 2019; Figure 6

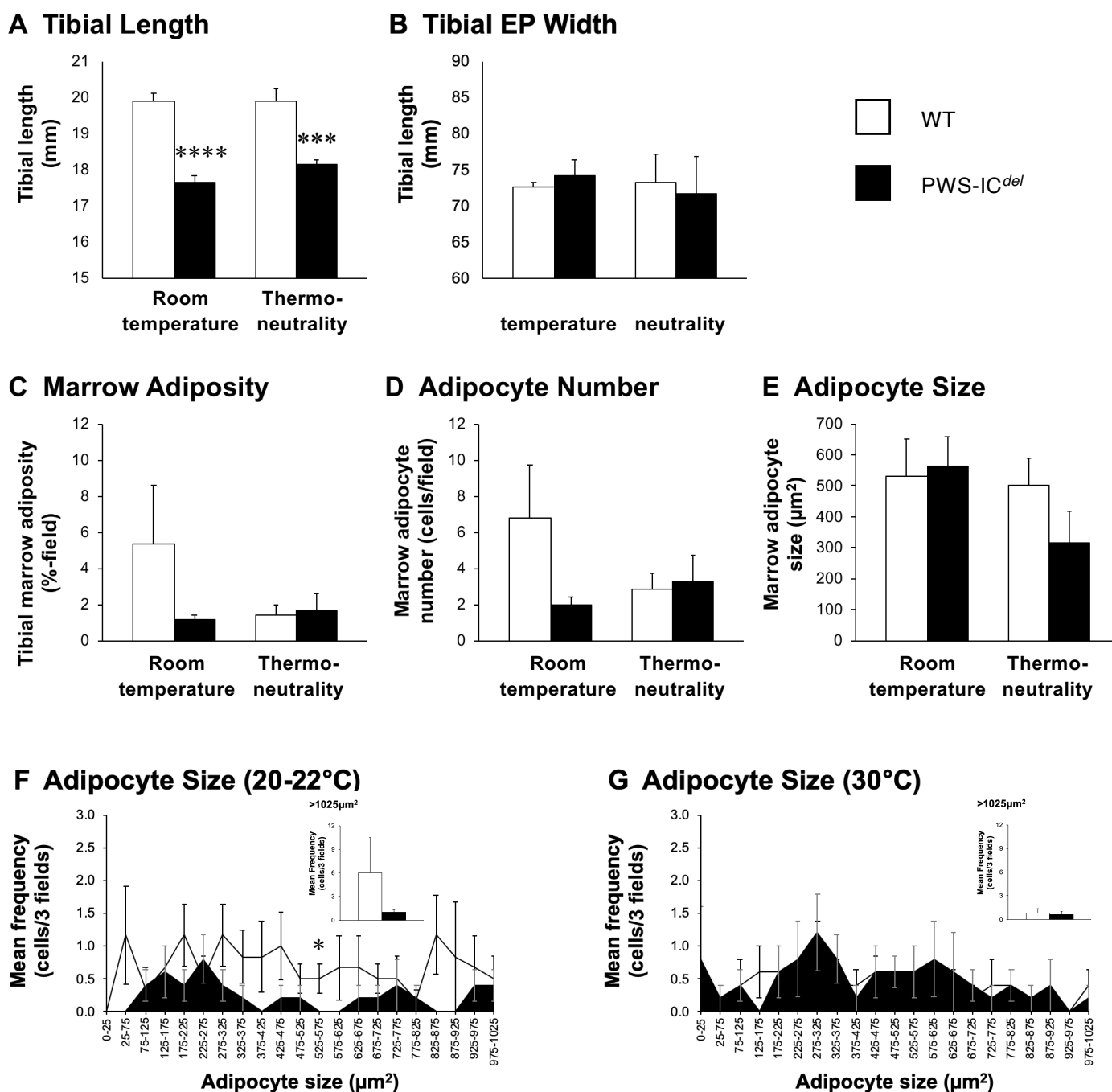


**Figure 6: Thermoneutrality has little effect on growth and marrow adiposity in PWS-IC<sup>del</sup> mice.** Tibial length (A), epiphyseal plate (EP) width (B), marrow adiposity (C), adipocyte number (D) and mean adipocyte size (E) were quantified in 6-15-month old male WT and PWS-IC<sup>del</sup> after being maintained at either standard ambient temperature (20-22°C) or thermoneutrality (30°C) for 9 weeks. Adipocyte size profiles are presented for standard ambient temperature (F) and thermoneutrality (G). Data shown are mean  $\pm$  SEM (n=6 (room temperature) and 5 (thermoneutrality)), with statistical comparisons performed by 1-way ANOVA and Bonferroni post hoc test (A-E; \*\*\*\* P<0.0001 vs room temperature (same genotype)) or unpaired Student's t-test (F & G; \* P<0.05 vs WT littermates (same temperature)).

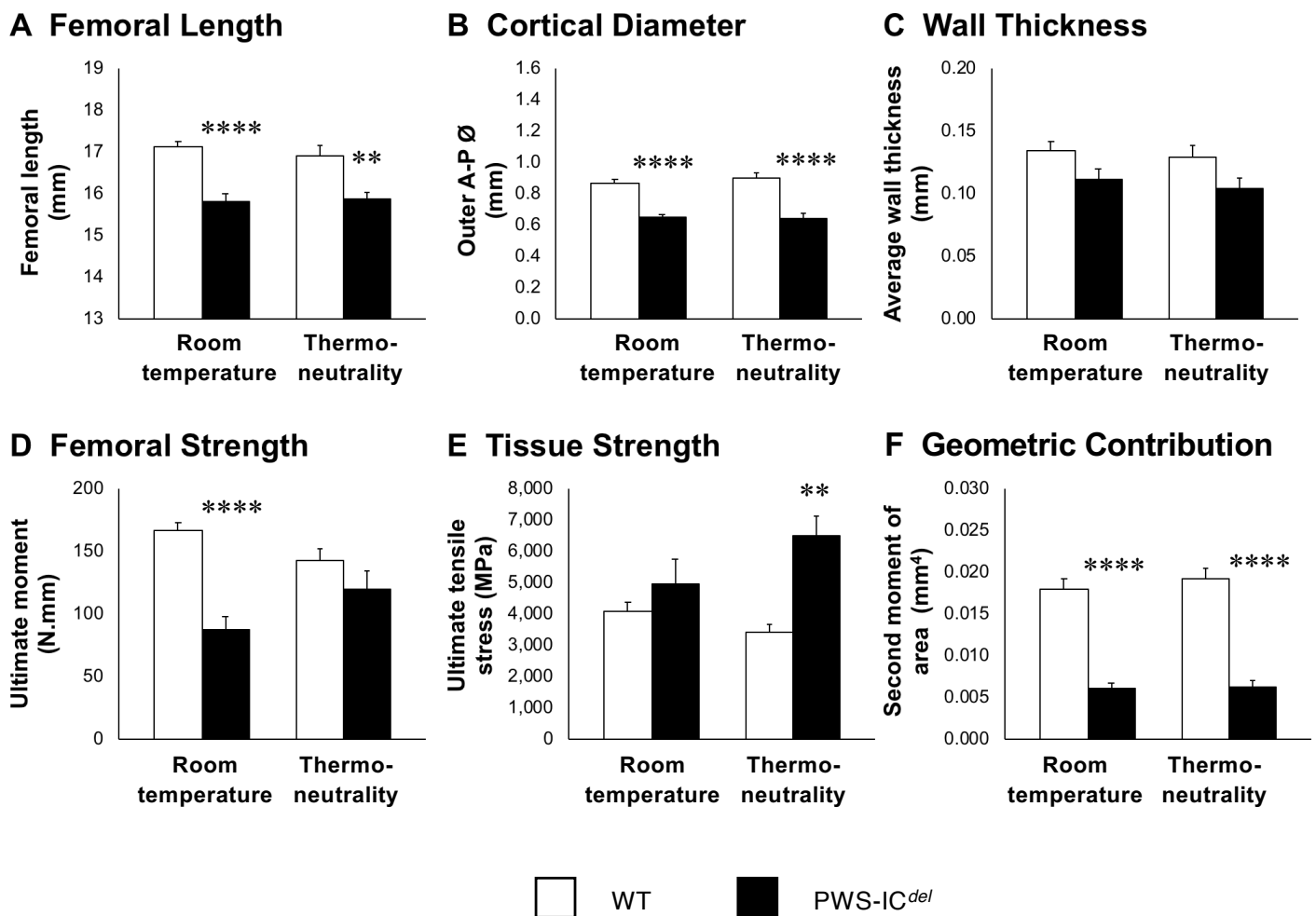


**Figure 7: Thermoneutrality has little effect on growth and marrow adiposity in PWS-IC<sup>del</sup> mice.** Tibial length (A), epiphyseal plate (EP) width (B), marrow adiposity (C), adipocyte number (D) and mean adipocyte size (E) were quantified in 6-15-month old male WT and PWS-IC<sup>del</sup> after being maintained at either standard ambient temperature (20-22°C) or thermoneutrality (30°C) for 9 weeks (n=6 (room temperature) and 5 (thermoneutrality)). Data shown are mean ± SEM, with statistical comparisons performed by 1-way ANOVA and Bonferroni post hoc test (\*\* $P < 0.01$ ; \*\*\*\* $P < 0.0001$  vs WT littermates (same ambient temperature)).